# Fabrication of Pt/Ru Nanoparticle Pair Arrays with Controlled Separation and their Electrocatalytic Properties

Björn Wickman,[†,*] Yvonne E. Seidel,[‡] Zenonas Jusys,[‡] Bengt Kasemo,[†] and R. Jürgen Behm[‡,*]

[†]Department of Applied Physics and Competence Centre for Catalysis, Chalmers University of Technology, SE-41296 Göteborg, Sweden, and [‡]Institute of Surface Chemistry and Catalysis, Ulm University, D-89069 Ulm, Germany

I n recent years we had developed novel nanostructured model electrodes, consisting of arrays of rather regularly arranged Pt nanodisks (diameter 50−150 nm, height 20−60 nm) supported on smooth glassy carbon substrates.[1] These electrodes were prepared by colloidal lithography (CL) techniques,[1,2] and were found to be stable in electrocatalytic reactions under enforced electrolyte flow, that is, in a flow cell.[3] Utilizing the possibility that the density and size of the nanodisks could be varied independently over a wide range in a controlled way, these electrodes were employed for systematic studies of transport effects in electrocatalytic reactions.[4−9] The transport conditions could be varied in a controlled way by changing either the size or density of the nanodisks or the flow rate of the electrolyte. In systematic investigations, performed under well-defined reaction and transport conditions in a flow cell, we could demonstrate that in electrocatalytic reactions involving the formation of incompletely reacted, reactive side products in addition to the fully reacted main product, the product distribution and hence the fraction of the stable product sensitively depends on the transport conditions, with an increasing content of the stable, fully reacted product with decreasing flow rate or with increasing density/coverage of the active nanodisks (decreasing space velocity[10]). Examples were the $O_2$ reduction reaction (ORR, $H_2O_2$ as reactive side product vs $H_2O$ as fully reduced product) or the oxidation of methanol (MOR, formaldehyde/formic acid vs $CO_2$) and formaldehyde (FOR, formic acid vs $CO_2$).[4−9] To explain these findings, a novel mechanism, the "desorption−readsorption−further reaction mechanism" was introduced.[5]

So far, Pt was used as the only active material throughout these studies. There

**ABSTRACT** Aiming at the investigation of spillover and transport effects in electrocatalytic reactions on bimetallic catalyst electrodes, we have prepared novel, nanostructured electrodes consisting of arrays of homogeneously distributed pairs of Pt and Ru nanodisks of uniform size and with controlled separation on planar glassy carbon substrates. The nanodisk arrays (disk diameter ≈ 60 nm) were fabricated by hole-mask colloidal lithography; the separation between pairs of Pt and Ru disks was varied from −25 nm (overlapping) via +25 nm to +50 nm. Morphology and (surface) composition of the Pt/Ru nanodisk arrays were characterized by scanning electron microscopy, energy dispersive X-ray analysis, and X-ray photoelectron spectroscopy, the electrochemical/electrocatalytic properties were explored by cyclic voltammetry, $CO_{ad}$ monolayer oxidation ("$CO_{ad}$ stripping"), and potentiodynamic hydrogen oxidation. Detailed analysis of the $CO_{ad}$ oxidation peaks revealed that on all bimetallic pairs these cannot be reproduced by superposition of the peaks obtained on electrodes with Pt/Pt or Ru/Ru pairs, pointing to effective Pt−Ru interactions even between rather distant pairs (50 nm). Possible reasons for this observation and its relevance for the understanding of previous reports of highly active catalysts with separate Pt and Ru nanoparticles are discussed. The results clearly demonstrate that this preparation method is perfectly suited for fabrication of planar model electrodes with well-defined arrays of bimetallic nanodisk pairs, which opens up new possibilities for model studies of electrochemical/electrocatalytic reactions.

**KEYWORDS:** model electrode · nanoparticle · platinum · ruthenium · hole-mask colloidal lithography · $CO_{ad}$ monolayer oxidation · hydrogen oxidation reaction

is, however, no principal reason ruling out the use of other metals or even alloys as active materials. The CL procedures applied for preparing the nanostructured electrodes do not allow, however, the fabrication of electrode surfaces containing the two metals in separate nanodisks, or even arrays with a regular arrangement of the two types of nanodisks. In addition to the principal interest in such kind of structures, this would be tempting, for example, for studies of different types of transport effects. For instance, there were a number of reports in recent years claiming that bimetallic catalysts were highly active, for instance, for methanol or CO oxidation, even if the two materials were present in separate monometallic nanoparticles, without direct contact between the two metals except for

cases where two different nanoparticles were accidentally touching.[11−16] In fact, catalysts with separate Pt and Ru nanoparticles (or electrodes consisting of a mix of Pt/C and Ru/C catalysts) were proposed to be even more active for the MOR than "normal" bimetallic PtRu/C catalyst with intermixed bimetallic nanoparticles.[11] (For a review on PtRu electrocatalysts see ref 17). This was attributed to boundary sites between Pt metal and Ru hydrous oxides.

To better understand the role of the metal–metal interaction in such systems, here specifically the Pt–Ru interaction, it would be highly desirable to have a model system where the separation between the Pt and Ru phases could be adjusted and varied in a controlled way.[13,16] This is the topic of the present paper, where we (i) introduce a modified hole-mask colloidal lithography (HCL)[18] process allowing us to produce ordered arrays of pairs of separated Pt and Ru nanodisks on a glassy carbon (GC) substrates and (ii) use these as model electrodes to explore the interaction between Pt and Ru nanostructures in electrochemical/-catalytic processes under well-defined reaction and transport conditions. The nanodisks had a diameter of about 60 nm and covered between 7 and 10% of the surface; samples with different separation between Pt and Ru nanodisks were prepared. After a brief description of the experimental procedures, we first describe the preparation of the nanostructured electrodes and characterize their structure and surface composition by scanning electron microscopy (SEM), energy dispersive X-ray (EDX) analysis, and X-ray photoelectron spectroscopy (XPS) before and after the electrochemical measurements. In the second part of the Results and Discussion section, the electrochemical and electrocatalytic properties of the nanostructured electrodes, as determined by base cyclic voltammetry (BCV), oxidation of a preadsorbed $CO_{ad}$ monolayer ("$CO_{ad}$ stripping"), and the hydrogen oxidation reaction (HOR) are evaluated and discussed. Finally, we briefly comment on the consequences of the present finding on the understanding of previously reported highly active PtRu catalysts with separate Pt and Ru nanoparticles.

## RESULTS AND DISCUSSION

**Fabrication and Physical Characterization of Nanodisk Pair Arrays.** Ordered Pt/Ru nanodisk pair arrays were fabricated on planar GC substrates using a variant of the HCL process, developed by Fredriksson et al.[18] Arrays of paired nanodisks with controlled separation between the disks in the pairs can be obtained by depositing the respective materials through the hole mask at two opposite, off-normal directions, in two subsequent deposition steps. To obtain pairs where the two nanodisks consist of different materials, one has to change the deposit material between the first and second deposition step. This is summarized schematically in Figure 1.
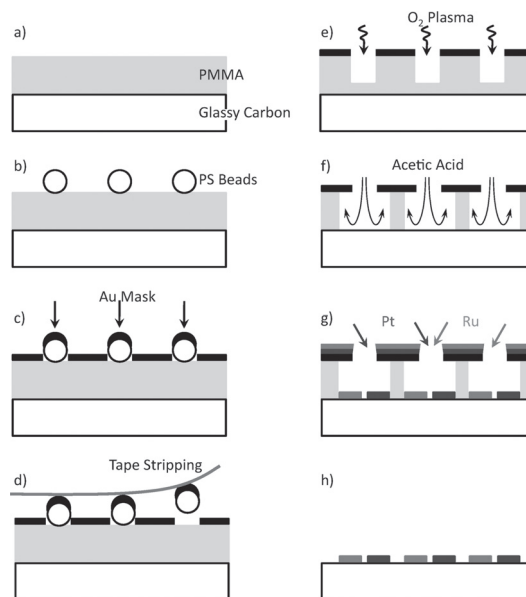


**Figure 1. Schematic illustration of the HCL process used to fabricate Pt/Ru nanoparticle arrays on polished GC electrodes. (a) A layer of PMMA is spin-coated onto the GC surface; (b) adsorption of PS beads; (c) evaporation of a Au mask; (d) tape stripping of PS beads, creating the hole mask; (e) oxygen-plasma etching of PMMA; (f) under-etching with acetic acid; (g) subsequent evaporation of Pt and Ru at opposing angles; (h) mask lift-off in acetone.**

The separation between the pairs can be varied by adjusting the deposition angle or by varying the height of the spacer layer carrying the Au mask. In the present work, we chose to vary the height of the poly-(methylmethacrylate) (PMMA) spacer layer for controlling the separation of the Pt and Ru nanodisk and keep the evaporation angle constant, since from experimental reasons this offered higher precision. PMMA layers of three different thicknesses, ∼70, ∼180, and ∼240 nm were used to obtain the overlapping (OL), small separation (SS), and large separation (LS) samples, respectively.

After preparation of the PMMA-supported Au hole mask (see Methods), an undercut in the PMMA layer, larger than the holes in the Au mask, must be provided in order to make room for the particle pairs. This was previously done by several minutes of exposure to an oxygen plasma.[18] In the present work, this process was not feasible since oxygen plasma very efficiently etches the GC substrate. Therefore, the samples were immersed in 100% acetic acid for 50 s to create an underetch with a diameter approximately three times larger than the holes in the Au mask. Pt and Ru nanodisks were deposited on the GC surface by subsequent e-beam evaporation (AVAC HVC-600) of Pt and Ru at +15 and −15° from the substrate surface normal, respectively. The pressure during evaporation was about 10⁻⁶ mbar and the distance between sample and source was 40 cm. It was demonstrated earlier that blurring effects in the deposition process are negligible;[19] Pt and Ru deposition is limited to the

size of the nanodisks. The evaporation of Pt and Ru was done through Al mask rings with a hole of 6 mm in diameter, resulting in an area covered by the nanoparticle pairs of 0.283 cm$^2$ centered on the GC substrate surface. Finally, the residual PMMA spacer and Au mask were lifted off in acetone.

The resulting samples are referred to according to material and deposition order in the following way: "1st material/2nd material", followed by an extension denoting the overlap or separation of the nanodisks in each pair: OL (second disk partly covers the first one by ~25 nm), SS (small separation of ~25 nm), or LS (large separation of ~50 nm).

In addition to Pt/Ru-OL, PtRu-SS, and Pt/Ru-LS nanodisk pairs, we included samples containing nanodisk pairs of a single material only, Pt/Pt-OL and Ru/Ru-OL, as well as a polycrystalline Pt sample (pc-Pt) and a polished and cleaned GC substrate (GC) as reference samples. The Pt/Pt-OL and Ru/Ru-OL samples were prepared in the same way as the overlapping Pt/Ru-OL sample, but evaporating the same material twice (at opposite angles, see above). This was done in order to keep the total metal content and disk coverage of the samples similar.

In the left column of Figure 2, we show SEM images of the different types of nanofabricated samples prior to the electrochemical measurements at low magnification, together with high magnification details in the insets. Pt nanodisks have a higher contrast and show up as brighter structures, while the Ru nanodisks are darker and slightly smaller in diameter (Pt nanodisks, ~63 nm; Ru nanodisks, ~53 nm). The size difference results from the fact that Pt was evaporated first, and similar differences were observed also on the Ru/Ru-OL sample. As Pt was deposited onto the mask, some material adsorbed on the edges of the holes and decreased the diameter of the holes in the protecting mask (for details see ref 18). The shape and size of the nanodisk pairs also depend on the interactions between the depositing material and the substrate and mask, respectively. For instance, there is a smaller difference in size between the first and second disk in the pairs on the Pt/Pt-OL sample compared to the Ru/Ru-OL sample.

The right-hand column of Figure 2 shows SEM images of the respective samples after the electrochemical evaluation. The diameters of the Pt and Ru nanodisks, separation/overlap, and the coverage of nanodisks were calculated from high magnification SEM images. At least 40 disk pairs on several images were measured in order to determine the diameters and separation/overlap for each sample. For the calculation of the Pt:Ru ratio and the geometric surface area, the nanodisks were assumed to have perfect cylindrical shape. The Ru disk diameters had decreased by about 16%, while the size of the Pt disks was more or less unchanged. The reasons and implications of the
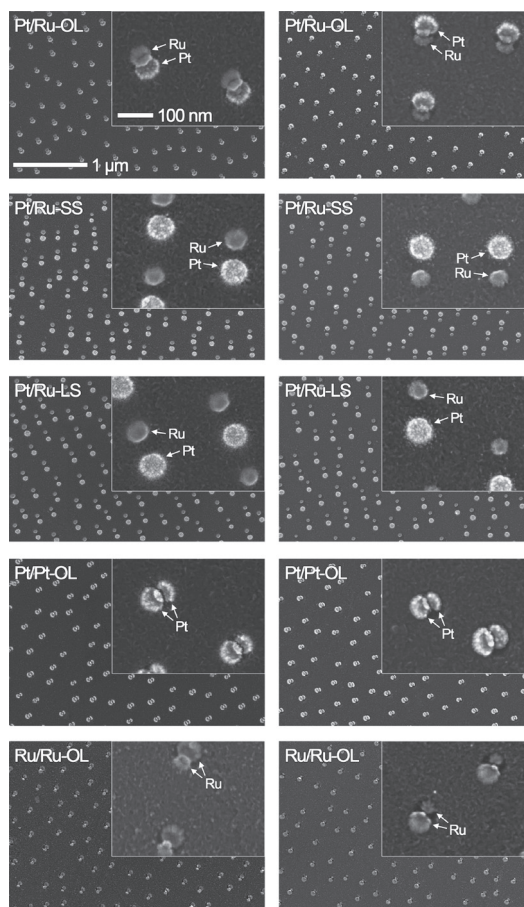


**Figure 2.** SEM micrographs of nanofabricated pair arrays before (left column) and after (right column) the electrochemical evaluation. High magnification SEM images are shown as insets for all samples. The scale bars shown in the top left image applies to all samples.

apparent loss of Ru will be discussed in more detail after presentation of the electrochemical data. The measured diameters, separation/overlap, and total coverage of Pt and Ru for all samples before and after the electrochemical measurements are summarized in Table 1.

EDX and XPS analysis was performed on all samples to obtain the (surface) composition. As the Ru(3d) core level peaks overlap with C(1s) peaks in the XPS analysis, the Ru(3p) together with Pt(4f) core level signals were used for the evaluation (see Supporting Information). The (surface) atomic fractions or surface area fractions (SEM) of Pt vs Ru for the Pt/Ru samples before and after the electrochemical analysis as determined by EDX, XPS, and SEM are presented in Table 2.

**Electrochemical Characterization.** Base cyclic voltammetry (BCV) was performed in N$_2$-purged 0.5 M H$_2$SO$_4$ before and after the electrocatalytic measurements including preadsorbed CO$_{ad}$ monolayer oxidation and continuous hydrogen oxidation. Representative current traces are shown in Figure 3. The Pt samples (Pt/Pt-OL and pc-Pt) show the typical uptake of underpotential

**TABLE 1. Size, Distribution, And Coverage of the Nanodisk Pair Arrays As Determined by SEM**

| | before electrochemistry measurements[a] | | | | after electrochemistry measurements[a] | | | |
|---|---|---|---|---|---|---|---|---|
| | disk diameter (nm) | | | | disk diameter (nm) | | | |
| sample | 1st disk[c] | 2nd disk[c] | separation[b] (nm) | total coverage (%) | 1st disk[c] | 2nd disk[c] | separation[b] (nm) | total coverage (%) |
| Pt/Ru-OL | 62 ± 3 | 52 ± 3 | −23 ± 4 | 7.3 ± 0.2 | 61 ± 4 | 45 ± 3 | −15 ± 3 | 6.8 ± 0.5 |
| Pt/Ru-SS | 64 ± 3 | 53 ± 4 | 25 ± 3 | 10.2 ± 0.7 | 62 ± 3 | 45 ± 3 | 27 ± 3 | 9.5 ± 0.7 |
| Pt/Ru-LS | 63 ± 4 | 53 ± 3 | 50 ± 4 | 10.2 ± 0.4 | 61 ± 4 | 44 ± 5 | 52 ± 4 | 9.5 ± 0.5 |
| Pt/Pt-OL | 63 ± 5 | 58 ± 3 | −23 ± 3 | 7.5 ± 0.2 | 55 ± 5 | 46 ± 4 | −21 ± 3 | 7.0 ± 0.3 |
| Ru/Ru-OL | 63 ± 4 | 41 ± 6 | −17 ± 4 | 6.4 ± 0.3 | 57 ± 5 | 34 ± 5 | −9 ± 9 | 5.6 ± 0.5 |

[a] The presented data are mean values from at least 40 nanodisk pairs for every sample, obtained from SEM images; the error margin is the standard deviation of all measured values. [b] Distance measured between the outer rims of paired disks. A negative value indicates overlapping disks. [c] On Pt/Ru samples, 1st disk is Pt and 2nd disk is Ru.

**TABLE 2. Composition of the Different Pt/Ru Samples before and after Electrochemical/Electrocatalytic Measurements As Determined by XPS, EDX, and SEM**

| | composition[a], $X_{Pt}$ (atomic %) | | | | | |
|---|---|---|---|---|---|---|
| | before electrochemistry measurements | | | after electrochemistry measurements | | |
| sample | XPS | EDX | SEM[b] | XPS | EDX | SEM[b] |
| Pt/Ru-OL | 56 ± 2 | 56 ± 2 | 52 ± 2 | 61 ± 3 | 67 ± 5 | 61 ± 3 |
| Pt/Ru-SS | 63 ± 5 | 58 ± 4 | 59 ± 4 | 71 ± 4 | 68 ± 5 | 65 ± 4 |
| Pt/Ru-LS | 64 ± 4 | 58 ± 5 | 59 ± 3 | 72 ± 5 | 69 ± 5 | 65 ± 5 |

[a] The numbers represent atomic % of Pt vs Ru.. [b] Projected area of perfect cylinders based on the data presented in Table 1.

deposited hydrogen (Pt−$H_{UPD}$ features) at potentials $E$ < 0.35 V (vs RHE). The active Pt surface area of these two samples was calculated from the $H_{UPD}$ charge in the cathodic scan, assuming a $H_{UPD}$ monolayer charge of 210 $\mu$C cm$^{-2}$ and a $H_{ad}$ coverage of 0.77[20] at the onset of bulk hydrogen evolution. This way, surface areas of 0.54 and 0.10 cm$^2$ were obtained for the pc-Pt and Pt/Pt-OL samples, respectively. The geometric Pt surface area, denoting the Pt surface area exposed to the electrolyte, was 0.283 cm$^2$ on pc-Pt. For the nanostructured samples, the geometric surface area corresponds to the sum of the surfaces of the individual free-standing Pt cylinders of ∼60 nm in diameter and 20 nm in height, resulting in 0.044 cm$^2$ for Pt/Pt-OL. Relating these values to the electrochemically active surface areas yields roughness factors (RF) of 1.9 for the pc-Pt and of 2.3 for the Pt/Pt-OL sample. The RF value for Pt/Pt-OL sample is in good agreement with previously reported data for HCL fabricated samples.[2,7,9] The larger pseudo-capacitive features in the double-layer region compared to the pc-Pt sample results from contributions from the GC support and are typical for Pt nanoparticle modified GC electrodes.[21,22]

The BCV traces for the Pt samples do not change significantly between the start (solid lines) and the end (dashed lines) of the electrochemical measurements,
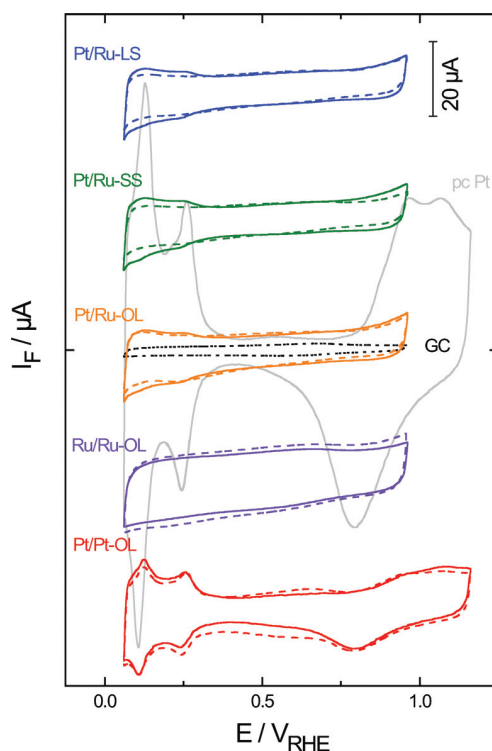


**Figure 3.** BCV curves recorded on nanostructured and reference electrodes (for assignments see figure) at the start of measurements (solid line) and after (dotted lines) electrocatalytic measurements including $CO_{ad}$-stripping and continuous hydrogen oxidation. Scan rate, 100 mV s$^{-1}$; electrolyte, $N_2$-purged 0.5 M $H_2SO_4$.

indicating that the samples are stable under experimental conditions, including continuous (enhanced) electrolyte flow. On the Pt/Pt-OL sample, the double layer currents were slightly higher after the electrochemical measurements, which is attributed to carbon corrosion during the excursions to higher potentials.

The BCV curves of the Ru/Ru-OL sample did not display typical $H_{UPD}$ features as observed for Pt, which is due to the fact that the Ru surface is still largely covered with O/OH surface species.[23,24] Similar to the Pt samples, there are no significant changes in the BCV curves between the start and end of the measurements,

indicating that the sample structure and composition remained more or less constant, and that this sample was also relatively stable. Accordingly, no evident particle loss could be seen from the SEM micrographs taken before and after the electrochemical measurements (Figure 2).

The three Pt/Ru samples exhibit similarly shaped BCV traces at the beginning of the measurements. Only weak Pt-$H_{UPD}$ peaks are seen at E < 0.35 V. Thus, the BCV response does not seem to be affected by the overlap or separation of Pt and Ru nanodisks. In contrast to the Pt or Ru electrodes, however, the shape of the BCV traces changed significantly during the electrochemical measurements, and the peaks in the $H_{UPD}$-region more or less disappeared (most pronounced on the Pt/Ru-LS and Pt/Ru-SS samples). At the end of the measurements, the BCV curves looked similar to the featureless shape of the Ru/Ru-OL sample. The reason for that can either be uptake of adsorbing contaminants from the electrolyte due to the lower anodic potential limit or modifications in the nanodisks induced by the electrochemical processes. The first explanation is implausible in view of the stable behavior of the Pt samples. Even though reference $CO_{ad}$ stripping experiments with an upper potential limit of $E = 0.96$ V on the Pt samples also showed a small decrease in the $H_{UPD}$-region in comparison to the same experiment with an upper potential limit of $E = 1.16$ V, it was, in this case, marginal. The second explanation appears more likely and this will be discussed in more detail at the end of the following section.

**$CO_{ad}$ Monolayer Oxidation.** Figure 4 presents data from preadsorbed $CO_{ad}$ monolayer oxidation measurements and a subsequent cyclic voltammogram carried out at a scan rate of 10 mV s$^{-1}$. During the first positive-going scan, $CO_{ad}$ preadsorbed at 60 mV is oxidized ("stripped") from the metal. For the Pt samples, this results in a prewave followed by a distinct and narrow stripping peak with a maximum located at ∼0.7 V for both the pc-Pt and the Pt/Pt-OL sample. Since the contribution of double-layer charging during the CO adlayer stripping measurements does not exceed 20% on pure Pt,[25−27] it is sufficient in a first approximation to use the BCV corrected $CO_{ad}$ oxidation charge to calculate the active Pt surface area of these two samples. This was done by assuming a $CO_{ad}$ monolayer charge of 420 $\mu$C cm$^{-2}$ and a $CO_{ad}$ saturation coverage of 0.75 monolayers.[1,9,28,29] The results obtained were in fairly good agreement with the active surface areas determined by $H_{UPD}$ charge formation (see Table S1, Supporting Information).

On the Ru/Ru-OL sample, we found a rather broad $CO_{ad}$ oxidation region, between ∼0.40 and 0.96 V instead of a sharp stripping peak. It is well-known that the intrinsic reaction rate for CO oxidation on polycrystalline Ru is much lower than on Pt, which results in a broader oxidation peak.[23,30−32] However, a $CO_{ad}$
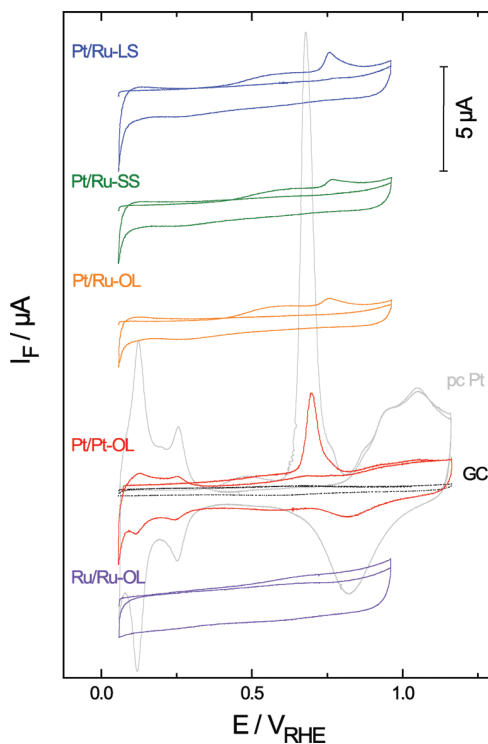


**Figure 4.** Preadsorbed $CO_{ad}$ monolayer oxidation on nanostructured and reference electrodes (for assignments see figure). Prior to $CO_{ad}$ monolayer oxidation, the electrodes were saturated with CO at 0.06 V for 5 min and afterward rinsed with CO-free base solution for around 20 min. Scan rate, 10 mV s$^{-1}$; electrolyte, $N_2$-purged 0.5 M $H_2SO_4$.

oxidation peak would still be expected, and it should start at a lower potential than on Pt if the Ru is in a metallic state.[23] The $CO_{ad}$ stripping response seen for the Ru/Ru-OL sample is similar to that presented in ref 33. Gasteiger et al.[23] pointed out that the latter was likely to result from an oxidized Ru surface. Additional $CO_{ad}$ stripping measurements on this sample were performed in a differential electrochemical mass spectrometry (DEMS) setup,[13,27,29] where the formation of $CO_2$ (m/z = 44) was monitored (Supporting Information, Figure S3). In the DEMS measurements, a broad $CO_2$ formation peak was observed between 0.5 and 1.0 V. Hence, indeed part of the Faradaic current shown in Figure 4 results from $CO_{ad}$ oxidation. Comparison of the partial Faradaic current generated by oxidation of $CO_{ad}$ to $CO_2$ ($I_F(CO_2)$) and the BCV corrected $CO_{ad}$ stripping signal demonstrates, however, that a significant part (about half) of the Faradaic current is due to double-layer charging and Ru oxidation on the Ru sample (see Supporting Information), in agreement with previously reported data.[34]

For the Pt/Ru pair samples, the $CO_{ad}$ oxidation started at roughly the same potential as on the Ru sample (∼0.4 V), but the increase in oxidation rate was much faster. Overall, the three Pt/Ru samples show essentially the same $CO_{ad}$ oxidation behavior. At higher potentials (∼0.75 V) there was a small peak of similar
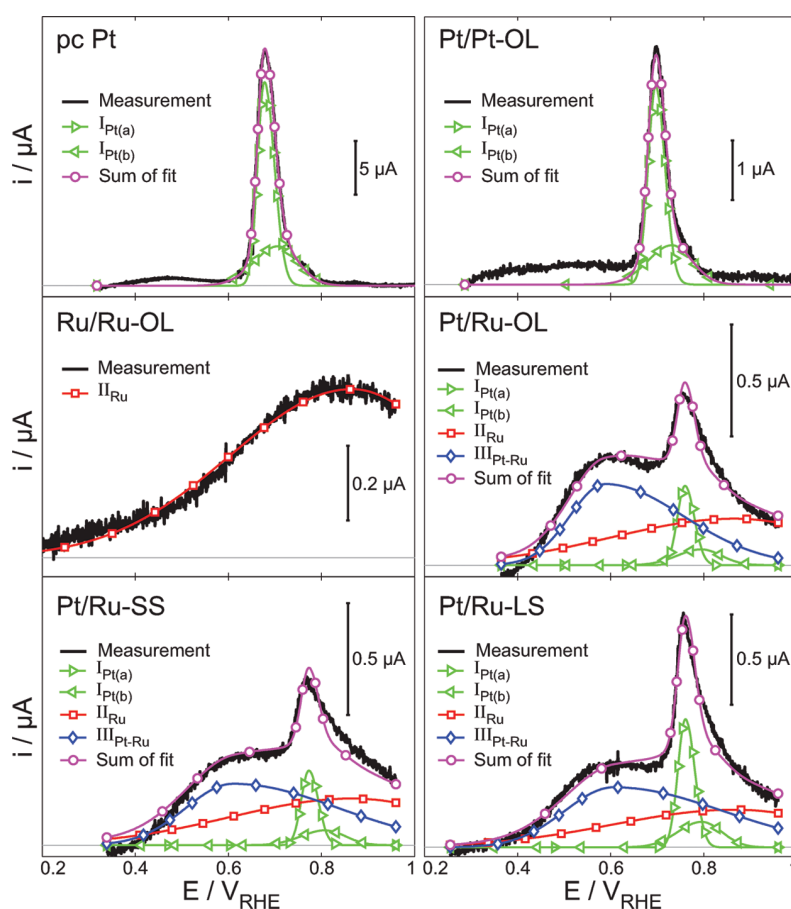
**Figure 5.** BCV subtracted preadsorbed $CO_{ad}$ monolayer oxidation current recorded at 10 mV s$^{-1}$ in $N_2$-purged 0.5 M $H_2SO_4$ and deconvolution of the corresponding contributions.

shape observed for all Pt/Ru samples. Compared to the Pt samples, the magnitude of the peak was significantly lower and the position of the maximum was shifted to slightly higher potentials. Most striking is that significant $CO_{ad}$ oxidation is observed at potentials between 0.5 and 0.7 V, where the Pt and Ru samples showed a rather low $CO_{ad}$ oxidation activity.

For a more quantitative examination of the $CO_{ad}$ stripping data and the role of Pt and Ru nanodisk separation, we tried to fit the BCV corrected $CO_{ad}$ stripping data by superposition of the peaks from $CO_{ad}$ stripping on Pt nanodisks and on Ru nanodisks. The latter were obtained by using the Pt/Pt-OL and Ru/Ru-OL reference samples. BCV corrected data were calculated by subtracting the second positive-going scan (BCV) presented in Figure 4, from the first one ($CO_{ad}$ stripping trace). As mentioned before, contributions from modified double-layer charging and Ru oxidation are not included in the BCV corrections. Nevertheless, $CO_{ad}$ oxidation provides a large fraction of the resulting current, and the BCV correction can be seen as a simplified *ansatz* and be used to examine trends on the different samples. For peak fitting we used asymmetric Gaussian functions, which can be motivated by the fact that (i) kinetic models usually predict

asymmetric stripping peaks,[35−37] and that (ii) an asymmetry was needed in order to get a good fit that could be related to the fractions of Pt and Ru on the samples.

The results of this approach are shown in Figure 5, and the values of the fitted parameters are presented in Table 3. We start with fitting the CO oxidation peaks obtained on the Pt samples. For the pc-Pt and the nanodisk Pt/Pt-OL sample, two peaks were needed for a good fit, a larger, narrow peak $I_{Pt(a)}$ at lower potentials (at 0.68 and 0.70 V for pc-Pt and Pt/Pt-OL, respectively) and a second, smaller and wider peak $I_{Pt(b)}$ at higher potentials (centered around 0.71 and 0.73 V for pc-Pt and Pt/Pt-OL, respectively). On both pc-Pt and Pt/Pt-OL, the charge in the second peak corresponds to about 34% of the total charge, indicating that the nature of the Pt surface is similar on these two samples. The presence of two different peaks might indicate that CO was adsorbed on two (or more) different types of sites, for instance, different Pt crystal phases.[36] The total charge of the two fitted peaks was in good agreement with the integrated $CO_{ad}$ stripping and $H_{UPD}$ charges (see Table S1, Supporting Information).

On Ru, the situation is different. Adsorbed CO suppresses the Ru oxidation at low potentials during the first positive-going scan. This will instead start with

**TABLE 3. Values of All Fitted Parameters for the Curves Shown in Figure 5,** [a]

**Sole Pt Samples**

| sample | peak $I_{Pt(a)}$ | | | | peak $I_{Pt(b)}$ | | | |
|---|---|---|---|---|---|---|---|---|
| | $Q$ ($\mu$C) | $E_m$ (V) | $\sigma$ | $a$ | $Q$ ($\mu$C) | $E_m$ (V) | $\sigma$ | $a$ |
| pc-Pt | 82.9 | 0.68 | 0.021 | 0.69 | 42.4 | 0.71 | 0.043 | 1.2 |
| Pt/Pt-OL | 16.0 | 0.70 | 0.020 | 0.82 | 8.3 | 0.73 | 0.043 | 1.2 |

**Sole Ru and Pt/Ru Samples**

| sample | peak $I_{Pt}$ | | | | peak $II_{Ru}$ | | | | peak $III_{Pt-Ru}$ | | | |
|---|---|---|---|---|---|---|---|---|---|---|---|---|
| | $Q$ ($\mu$C) | $E_m$ (V) | $\sigma$ | $a$ | $Q$ ($\mu$C) | $E_m$ (V) | $\sigma$ | $a$ | $Q$ ($\mu$C) | $E_m$ (V) | $\sigma$ | $a$ |
| Ru/Ru-OL | | | | | 26.6 | 0.87 | 0.218 | 1.2 | | | | |
| Pt/Ru-OL | 1.7 | 0.76 | 0.020 | 0.82 | 13.3 | 0.87 | 0.218 | 1.2 | 11.8 | 0.59 | 0.168 | 0.45 |
| Pt/Ru-SS | 1.6 | 0.77 | 0.020 | 0.82 | 13.3 | 0.87 | 0.218 | 1.2 | 11.9 | 0.61 | 0.226 | 0.45 |
| Pt/Ru-LS | 3.4 | 0.76 | 0.020 | 0.82 | 13.3 | 0.87 | 0.218 | 1.2 | 15.0 | 0.61 | 0.234 | 0.45 |

[a] $Q$ is the charge, $E_m$ is the peak position, $\sigma$ is the FWHM, and $a$ is the asymmetry factor.

the onset of $CO_{ad}$ oxidation, and therefore the true $CO_{ad}$ oxidation current cannot be assessed by simply subtracting the BCV.[34,38] Therefore, the pure $CO_{ad}$ oxidation current for the Ru/Ru-OL sample was obtained from DEMS measurements, where the $CO_2$ formation current ($m/z = 44$) was monitored (see Supporting Information). The results showed that approximately 50% of the Faradaic current is generated from $CO_{ad}$ oxidation. However, for fitting the $CO_{ad}$ stripping current on the Ru/Ru-OL sample, we chose to not distinguish between $CO_{ad}$ oxidation and Ru oxidation, but instead combine these contributions in a single peak, which is given by the BCV subtracted data. This could be fitted rather well by a single, broad peak with a maximum at around 0.87 V (peak $II_{Ru}$).

For the three different Pt/Ru samples, we started the fitting by using the peaks obtained for the Pt/Pt-OL and Ru/Ru-OL samples. It was evident that it is not possible to reproduce the experimental data by any superposition of these Pt- and Ru-related peaks. Most obviously, we had to shift the $I_{Pt(a)}$ peak to slightly higher potential to make it overlap with the distinct peak evident in the measured data. Therefore we decided to shift the second Pt-related $CO_{ad}$ stripping peak, $I_{Pt(b)}$, by a similar amount and keep the charge ratio between the two peaks constant, but allow the total charges in these peaks to vary. The shape controlling parameters (i.e., full width at half maximum (fwhm) and asymmetry factor) were not allowed to vary. The $II_{Ru}$ peak was allowed to vary in intensity, but the other characteristics were maintained (see Table 3). Its charge was restricted to be no greater than half of that obtained from the Ru/Ru-OL sample, since the Ru fraction of the total metal surface on all Pt/Ru samples was about 50% of that for the Ru/Ru-OL electrode. The difference between these three peaks and the measured $CO_{ad}$ stripping current can be described well by a fourth peak. This peak (peak $III_{Pt-Ru}$) is proposed to

represent the contribution from interacting Pt−Ru. It is located more than 100 mV negative compared to the main stripping peak on Pt ($I_{Pt(a)}$), and its shape corresponds rather well to the stripping peaks obtained on Pt−Ru alloys.[13,23,34,39,40] The characteristics of this peak, that is, the fitted peak positions, fwhm, and asymmetry factor are similar (within the accuracy of the measurement) for the three different Pt/Ru samples (see Table 3). (A qualitative comparison of the sum of the fitted peaks and the experimentally determined $CO_{ad}$ stripping charges is given in Table S1 in the Supporting Information.)

It is important to note that the data for the Pt/Ru samples could only be reproduced if in addition to contributions from the Pt and Ru nanodisks a further peak was included, whose characteristics resemble those of PtRu (surface) alloys.[17] The comparison of the individual peak areas on the three Pt/Ru samples with the composition of Pt vs Ru (presented in Table 3) revealed that the combined charge in peaks $I_{Pt}$ (corresponding to Pt) and $III_{Pt-Ru}$ (corresponding to Pt/Ru surface-alloy) agrees with the measured fractions of Pt (presented in Table 2). The combined charge of peaks $I_{Pt}$ and $III_{Pt-Ru}$ constituted 52, 52, and 60% of the total charge for the Pt/Ru-OL, Pt/Ru-SS, and Pt/Ru-LS electrodes, respectively. Apparently, the configuration of the Pt and Ru particles in the pairs, that is, the separation between Pt and Ru nanodisks, does not change the $CO_{ad}$ oxidation response significantly. In particular, peak $III_{Pt-Ru}$, which was assigned to interacting Pt and Ru, is present and of comparable size also for the separated pairs. There are two possible explanations for this behavior: (i) a bifunctional mechanism could be responsible for peak $III_{Pt-Ru}$ if the communication between Pt and Ru phases is very long ranged (the separation between Pt and Ru on the Pt/Ru-LS sample was ~50 nm) and (ii) small amounts of Ru are dissolved during the initial electrochemical steps (cleaning, BCV, and HOR), during excursions to higher potentials,[41] and subsequently redeposited on the Pt

nanodisks. The first explanation would imply that adsorbed oxygenated surface species formed on the Ru nanodisks can spill over to the GC support and move over the surface to the Pt nanodisks. Even if this process cannot be ruled out, we consider it to be highly unlikely. Furthermore, contributions from this process would be expected to change heavily with increasing separation, which is not observed experimentally. The second possibility would result in partly Ru surface-decorated Pt nanodisks. It has indeed been shown that deposition of small amounts of Ru, in the range of fractions of a monolayer, on a Pt surface can shift the onset of CO oxidation to lower potentials and give rise to $CO_{ad}$ oxidation responses similar to those of Pt−Ru alloys.[42,43] The SEM evaluation after the electrochemical measurements (Figure 2 and Table 1) revealed that the Ru particles had decreased in size, probably due to Ru corrosion at the high potentials during sample cleaning and BCV.[41] Hence, it is likely also from these observations that a small fraction of the dissolved Ru is redeposited on the Pt nanodisks. This is supported also by the observed loss of Pt−$H_{UPD}$ features on the Pt/Ru samples during the course of the measurements (Figure 3), which can be explained by a "poisoning" of the Pt surface by Ru. In general, Ru redeposition should depend on the distance from the Ru nanodisk as Ru source. The characteristic length scale for the lateral decay in Ru redeposition, however, should be much larger than the typical separation of Pt and Ru nanodisks, considering the experimental parameters such as cell volume or diffusion constant of dissolved $Ru^{3+}$ ions. This results in an almost homogeneous Ru deposition over the entire electrode surface. Hence, although we do not have any direct evidence for Ru redeposition on Pt, we consider this as the most likely explanation of the modified electrochemical behavior of the Pt nanodisks based on the sample structure and the data presented above. Accordingly, we propose that the electrochemical treatment preceding the $CO_{ad}$ stripping experiments resulted in dissolution of Ru and its partial redeposition on Pt nanodisks. Similar Ru dissolution and redeposition processes can also explain previous reports of highly active PtRu catalysts, which were based on nonalloyed, separate Pt and Ru nanoparticles.[13,16]

**Hydrogen Oxidation.** Continuous measurements of the hydrogen oxidation reaction (HOR) were carried out in $H_2$-saturated electrolyte by scanning the potential (10 mV s$^{-1}$) from the onset of $H_2$ evolution to 0.76 V at three different flow rates, 1, 10, and 25 $\mu$L s$^{-1}$. Representative results obtained at 25 $\mu$L s$^{-1}$ are presented for all samples in Figure 6. The inset in Figure 6 shows the correlation between the electrolyte flow rate and the transport limited currents for all samples.[44] In contrast to the BCV and the $CO_{ad}$ stripping measurements, the HOR is obviously affected by reactant transport and should, hence, be sensitive to changes in the diffusion characteristics in the measurements on the nanostructured
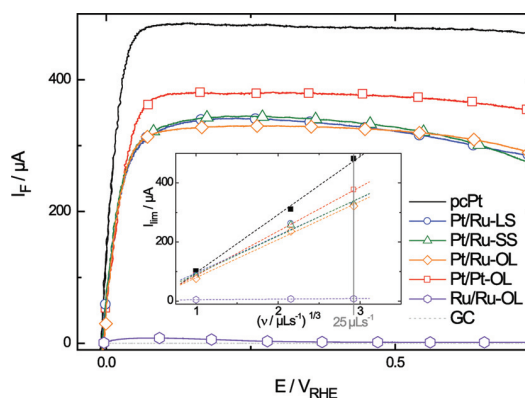


**Figure 6.** Continuous hydrogen oxidation (HOR) during positive-going scan on nanostructured and reference samples measured with an electrolyte flow rate of 25 $\mu$L s$^{-1}$. Scan rate, 10 mV s$^{-1}$; electrolyte, $H_2$-saturated 0.5 M $H_2SO_4$. The inset shows the flow rate dependence of limiting currents in a thin-layer flow cell (after Weber and Long[44]).

samples. The HOR on Pt in acidic electrolyte is one of the fastest known electrochemical reactions and proceeds almost without activation.[45] As a consequence, the current is almost always limited by mass transport of $H_2$ to the Pt surface already at potentials greater than 0.1 V. Figure 6 shows that the transport limited current for the pc-Pt sample was between 1.3 (Pt/Pt-OL) and 1.5 (Pt/Ru-samples) times higher than that on the Pt containing nanostructured samples. This is not surprising, considering that the Pt coverage was 100%, whereas on the nanostructured samples the Pt coverages are 3.9% (Pt/Ru-OL), 6.1% (Pt/Ru-SS and Pt/Ru-LS) and 7.5% (Pt/Pt-OL). However, the transport limited current densities, normalized to the Pt coverage, were much higher on the nanostructured samples than on the pc-Pt electrode. These observations are in good agreement with simple ideas about diffusion above arrays of ultramicroelectrodes (UMEs) on a planar support, where decreasing the size/increasing the separation between the UMEs gives rise to different mass transport conditions, or with the findings of an increased mass transport to a single Pt UME.[46,47] On a flat Pt surface, such as the pc-Pt sample, the diffusion profile perpendicular to the surface is uniform over the sample ("planar diffusion"), reaching zero concentration at the Pt surface. On the nanostructured samples, there is instead a hemispherical diffusion zone around each nanodisk ("hemispherical diffusion") and thus the mass transport to each disk is higher than the corresponding transport to a similar-sized area on the pc-Pt.[5,48−51] For intermediate separations between the nanodisks, diffusion is dominated by hemispherical diffusion close to the electrode surface, while further away overlap between neighboring hemispheres results in a planar diffusion front.[5,48−51] Since the latter is transport limiting, the total transport to the surface will not change as long as planar diffusion is dominant, resulting in constant transport limited currents and a linear increase of the transport limited (geometric)

current density. Only at further increased distances between the nanodisks, where planar diffusion is no more dominant, these relations break down. This is another important property of this type of nanostructured samples, which can be utilized to decouple mass transport effects from electrochemical reactions. Similar findings were reported previously for a number of reactions on similar types of nanostructured Pt/GC electrodes, including the oxygen reduction reaction,[4,5] CO adsorption, and oxidation,[52] and formaldehyde[9] as well as methanol oxidation,[7] but such kinds of transport effects have also been observed on thin-film catalyst electrodes.[53] Investigating the HOR in a RDE setup at various rotation rates, Wang *et al.* demonstrated that the high activity of metallic Pt nanoparticles (in a carbon supported Pt catalyst) for the HOR is retained for a catalyst where small Pt clusters are deposited on Ru nanoparticles (*e.g.*, PtRu$_{20}$, $^1/_9$ monolayer of Pt spontaneously deposited on metallic Ru nanoparticles).[54]

The HOR characteristics are very different on the Ru electrode. The intrinsic catalytic activity for HOR is several orders of magnitude lower on Ru compared to Pt.[55] This is reflected also by the present data. On Ru, the HOR current reaches a kinetically limited maximum around 0.2 V and then decreases to almost zero at potentials around 0.35 V. This is because the OH$_{ad}$ formation/surface oxidation on Ru already starts at around 0.2 V and progressively develops with increasing potentials, which results in increasing surface blocking of the Ru surface.[32,54,56−59] The (purely kinetically limited) maximum HOR current on the Ru/Ru-OL sample was about 2% of the transport limited current on the Pt/Pt-OL sample; the actual difference between the inherent activities of Pt and Ru, however, is much bigger. It would be given by comparing the kinetically limited currents at 0.2 V of both electrodes.

Finally, the Pt/Ru pair samples show a lower mass transport limited current and a more pronounced decay at higher potentials compared to Pt/Pt pair sample (Figure 6). The first observation can be rationalized by the lower density of active (Pt) nanodisks, since half of them are substituted by inactive Ru nanodisks. Apparently, the density is below the critical value where the transport characteristics start to deviate from planar diffusion to a homogeneous active surface, and where a further lowering of the nanodisk density is directly visible in the transport limitations.[5,52] In addition, the surface of the Pt nanodisks is probably modified by redeposited Ru (see above), which is likely to reduce the HOR activity at more anodic potentials due to enhanced OH$_{ad}$ formation. The resulting kinetic limitations can explain the more pronounced decay of the Faradaic current at more anodic potentials observed on the Pt nanodisks.

Overall, the two-dimensional ultramicroelectrodes arrays consisting of pairs of metal nanodisks with controlled and adjustable separation have been demonstrated to be an excellent experimental platform for model studies of proximity and transport effects in electrocatalytic reactions, which are hardy accessible in a more realistic system, and not even in model studies using carbon supported nanoparticle catalysts, because of the ill-defined separation between different types of nanoparticles therein. For instance, in previous experiments using catalysts prepared by deposition of preformed Pt and Ru nanoparticles on a highly disperse carbon Vulcan XC72 support, where intermixing of the two metals in the nanoparticles could be excluded, it could not be ruled out that subsequent conditioning of the catalysts resulted in enhanced contact of the Pt and Ru nanoparticles, which could explain the PtRu-like CO$_{ad}$ stripping characteristics observed also in that study.[13] Such effects can clearly be ruled out in the present model systems, where the separations between Pt and Ru nanodisks in the electrochemical measurements are well-defined, and where surface modification of the Pt nanodisks by Ru redeposition represents the only realistic explanation for the experimental findings. In general, further information can be obtained by exploiting the possibility of varying the separation between the different nanodisks in the pairs in a controlled way. Finally it should be noted that similar studies are possible also for three or four different metals, which would allow detailed model studies also for ternary and quaternary metal catalysts.

## CONCLUSIONS

The modified hole-mask colloidal lithography nanofabrication method developed in this study has successfully been employed to fabricate model electrodes covered by homogeneously distributed Pt and Ru nanodisk pair arrays with controlled separation. The possibility to precisely control the separation of bimetallic phases enables fabrication of model systems that are ideally suited for studying proximity and transport effects between phases in bimetallic systems. This relatively fast and simple procedure is capable of covering areas of several cm$^2$ with well-defined nanoparticles and should find applications also outside of electrocatalysis.

Pt and Ru pair arrays of nanodisks ($\sim$60 nm in diameter) with varied separation, deposited on GC substrates, were prepared and employed to explore possible interactions and between Pt and Ru in catalyst systems with separated Pt and Ru nanoparticles. Before and after electrochemical/catalytic measurements, the morphology and (surface) composition of the electrodes was characterized by SEM, EDX, and XPS.

Preadsorbed CO$_{ad}$ monolayer oxidation ("CO$_{ad}$ stripping") experiments revealed that the reaction behavior cannot be explained by superposition of the CO$_{ad}$ stripping peaks from Pt and Ru nanodisks as seen on Pt/Pt or Ru/Ru samples, but requires an additional contribution, which replaces much of the contribution characteristic for reaction on Pt

nanodisks. The data show an additional activity for $CO_{ad}$ oxidation in the potential range of 0.5 to 0.7 V, and fitting shows that an additional peak (peak $III_{Pt-Ru}$), with a maximum around 0.6 V, was required to reproduce the experimental data. This peak, which must result from interactions between Pt and Ru, closely resembles that observed for $CO_{ad}$ oxidation on Pt−Ru alloys and Ru decorated Pt surfaces. Since the contributions from the individual peaks were essentially the same for all three Pt/Ru samples, regardless of overlap or separation between the Pt and Ru nanodisks, and since the combined area of peak Pt- and Pt−Ru-related peaks ($I_{Pt(a)}$, $I_{Pt(b)}$, $III_{Pt-Ru}$) relative to that of the Ru-related peak ($II_{Ru}$) agreed well with the ratio of Pt vs Ru on the samples determined by spectroscopic/microscopic means, peak $III_{Pt-Ru}$ seems to originate from $CO_{ad}$ stripping on Pt nanodisks. It is explained by surface modification of the Pt surface, by redeposition of Ru which was dissolved from Ru nanodisks during electrochemical treatment. Ru decorated Pt surfaces in turn are well-known for their high activity in CO oxidation. This interpretation is supported also by the observed loss of the characteristic $H_{UPD}$ features on the Pt/Ru samples with ongoing measurements. Another possible process, spillover of adsorbed oxyspecies from Ru to Pt nanodisks, is not only highly unlikely, but can be ruled out also from the absence of effects caused by the varied separation between Pt and Ru nanodisks in the experimental data. Similar processes, dissolution, and subsequent redeposition of Ru during electrochemical processing are proposed also as origin for the high activity of PtRu catalysts based on separate Pt and Ru nanoparticles.

As expected from the high activity of Pt for hydrogen oxidation, the HOR experiments do not show any indication of long-range Pt−Ru interactions. The Faradaic current is dominated by hydrogen oxidation over the remaining Pt surface areas. The lower mass transport limited current on the Pt/Ru electrodes compared to Pt/Pt electrodes mainly reflect the lower density of highly active Pt nanodisks in the Pt/Ru model systems. Surface modification by redeposited Ru may by responsible for a kinetically limited decay at more anodic potentials, which is more pronounced on Pt/Ru than on Pt/Pt pair electrodes.

The results clearly demonstrate that the modified HCL route described in this work is perfectly suited for the fabrication of planar model electrodes with well-defined arrays of bimetallic nanodisk pairs or multi-metallic arrangements, which opens up new possibilities for model studies of electrochemical/-catalytic reactions, for example, for studying mechanistic proximity and/or transport effects in fuel cell relevant electrocatalytic reactions.

## METHODS

**Details of Sample Fabrication.** Prior to the deposition of the Pt/Ru nanodisk pair arrays, the glassy carbon (GC) substrates (9 mm diameter, Sigradur G from Hochtemperatur Werkstoffe GmbH) were polished to a mirror finish with alumina slurry down to 0.3 $\mu$m grid and thereafter cleaned by immersion in 5 M KOH and subsequently in concentrated $H_2SO_4$ solution. The samples were rinsed in Millipore Milli-Q water (resistivity >18 M$\Omega$ cm) before and after the immersions, and finally dried in a flowing $N_2$ stream.

The PMMA/Au hole-mask was prepared by spin-coating 2% PMMA in anisole at 3000 rpm to obtain the 70 nm spacer layer; 4% PMMA at 5000 and 3000 rpm were used for the 180 and 240 nm layers, respectively. The films were cured on a hot-plate at 170 °C for 10 min to evaporate solvent residues before a short oxygen plasma treatment (PlasmaTherm Batch-Top, 50 W, 5 s) was performed in order to increase the hydrophilicity of the surface. Then a solution containing positively charged polyelectrolyte (polydiallyldimethylammonium (PDDA), Sigma Aldrich, 0.2 wt % in Milli-Q water) was pipetted onto the PMMA film, followed by careful rinsing with Milli-Q water and blow-drying in a $N_2$-stream. In the next step, a water suspension containing negatively charged, 80 nm size (diameter) polystyrene (PS) particles (sulfate latex, Invitrogen, 0.2 wt % in Milli-Q water) was pipetted onto the surface, followed by rinsing and drying of the samples. Then an oxygen plasma resistant 20 nm Au film was thermally evaporated (Edwards HPTS) onto the sample surface and the PS beads were removed by tape stripping (SWT-10 tape, Nitto Scandinavia AB), leaving a Au hole-mask on the surface. The exposed PMMA in the holes left by the PS spheres was etched just down to the GC substrate surface using oxygen plasma.

**Physical Characterization.** Scanning electron microscopy (SEM), using a LEO Ultra 55 FEG (Zeiss Instruments) with an accelerating voltage of 10 kV, was employed to evaluate the morphology of the nanostructured electrodes. Energy dispersive X-ray (EDX, Oxford Inca System) analysis was performed in the SEM instrument simultaneously. The EDX spectra were analyzed using Oxford Instruments INCA software. X-ray photoelectron spectroscopy (XPS, Perkin-Elmer PHI 5000C ESCA system) was performed employing monochromatic Al−K$\alpha$ radiation at 45° takeoff angle. Standard sensitivity factors as given in ref 60 were used for determining the surface composition by XPS analysis via the Pt($4f_{7/2}$) and the Ru($3p_{3/2}$) signals; the area of the Pt($4f_{7/2}$) peak was estimated to be $^4/_7$ of that of the total Pt(4f) peak.

**Electrochemical Measurements.** The electrochemical characterization of the nanostructured electrodes was carried out in a thin-layer flow cell.[61] The GC substrate carrying the Pt and Ru nanodisk arrays, which served as working electrode, was pressed onto the main compartment of the thin-layer flow cell via a double layer of parafilm. Two Pt counter electrodes were connected to the cell via separate ports at the inlet and outlet of the cell. The reference electrode (saturated calomel electrode, SCE) was connected through a Teflon capillary at the outlet of the cell. All potentials, however, are reported vs that of the reversible hydrogen electrode (RHE). The potential was controlled using a bipotentiostat from Pine Instruments. Supporting electrolyte (0.5 M $H_2SO_4$) was prepared from Millipore Milli-Q water and ultrapure sulfuric acid (Merck, suprapur), and purged continuously with $N_2$. For CO adsorption, the base solution was saturated with CO (Messer-Griesheim, N 4.7), for hydrogen oxidation measurements high-purity $H_2$ (MTI Gase, N 5.7) was used instead. The electrolyte flow was driven by the hydrostatic pressure of the electrolyte in the supply bottle and controlled via a valve installed at the outlet of the cell.

Analogous to previous measurements on nanostructured Pt/GC electrodes,[1,2] the nanostructured electrodes were cleaned by repetitive rapid potential cycling within a preset potential window (0.06−1.36 V for the Pt and pure GC samples,

and 0.06−0.96 V for the Ru containing samples) in order to remove organic contaminations adsorbed on the electrode surface during sample preparation or picked up during sample transfer. This treatment was continued until reaching a stable CV trace. HOR measurements were carried out in $H_2$-saturated electrolyte by scanning the potential at 10 mV s$^{-1}$ between the onset of $H_2$ evolution and 0.76 V. $CO_{ad}$ stripping was conducted by holding the potential at 0.06 V and adsorbing CO from CO-saturated electrolyte for 5 min, followed by thorough rinsing with CO-free electrolyte for at least 20 min before starting the positive-going scan ($CO_{ad}$ oxidation), followed again by two full potential cycles in CO-free electrolyte (BCV). $CO_{ad}$ stripping was performed at four different scan rates: 10, 20, 50, and 100 mV s$^{-1}$. All measurements were carried out at room temperature.

**Fit of the $CO_{ad}$ Oxidation Current Peaks.** An asymmetric Gaussian function was used to describe the individual peaks for fitting the potentiodynamic $CO_{ad}$ oxidation data. For each peak, $i$, the following general expression was used to describe the current ($j$):

for $E \leq E_m$:

$$j_i = \frac{2Q_i v}{\sqrt{2\pi\sigma_i^2}(1+a_i)} \exp\left[-\frac{(E-E_{m,i})^2}{2\sigma_i^2 a_i^2}\right]$$

for $E > E_m$:

$$j_i = \frac{2Q_i v}{\sqrt{2\pi\sigma_i^2}(1+a_i)} \exp\left[-\frac{(E-E_{m,i})^2}{2\sigma_i^2}\right]$$

where $E$ is the electrode potential, $Q$ is the peak area (equivalent to the $CO_{ad}$ oxidation charge), $v$ is the scan rate, $E_m$ is the potential for the maximum current, $\sigma$ is the fwhm, and $a$ is the asymmetry factor. The function above was used for fitting the experimental data by fitting $Q$, $E_m$, $\sigma$, and $a$ using the function *lsqnonlin* in Matlab for 1−3 different peaks. In some cases, some of the parameters were fixed (see main text).

*Supporting Information Available:* EDX analyses of the nanostructured samples before the electrochemical evaluation, XP spectra recorded on the as prepared Pt/Ru-OL sample (overview spectrum, and details of the C(1s)/Ru(3d), the Pt(4f), and the Ru(3p) region), and DEMS measurements of preadsorbed $CO_{ad}$ monolayer oxidation on the Ru/Ru-OL as well as a table comprising the $H_{UPD}$ and $CO_{ad}$ oxidation charges, respectively, and the sum of the fitted charges from the deconvolution This material is available free of charge *via* the Internet at http://pubs.acs.org.

## REFERENCES AND NOTES

1. Gustavsson, M.; Fredriksson, H.; Kasemo, B.; Jusys, Z.; Jun, C.; Behm, R. J. Nanostructured Platinum-on-Carbon Model Electrocatalysts Prepared by Colloidal Lithography. *J. Electroanal. Chem.* **2004,** *568*, 371–377.
2. Seidel, Y. E.; Müller, M.; Jusys, Z.; Wickman, B.; Hanarp, P.; Kasemo, B.; Hörmann, U.; Kaiser, U.; Behm, R. J. Nanostructured, Glassy Carbon Supported Pt/GC Electrodes: The Presence of Secondary Pt Nanostructures, and How to Avoid Them. *J. Electrochem. Soc.* **2008,** *155*, K171–K179.
3. Seidel, Y. E.; Lindström, R.; Jusys, Z.; Gustavsson, M.; Hanarp, P.; Kasemo, B.; Minkow, A.; Fecht, H. J.; Behm, R. J. Stability of Nanostructured Pt/GC Electrodes Prepared by Colloidal Lithography. *J. Electrochem. Soc.* **2008,** *155*, K50–K58.
4. Schneider, A.; Colmenares, L.; Seidel, Y. E.; Jusys, Z.; Wickman, B.; Kasemo, B.; Behm, R. J. Transport Effects in the Oxygen Reduction Reaction on Nanostructured, Planar Glassy Carbon Supported Pt/GC Model Electrodes. *Phys. Chem. Chem. Phys.* **2008,** *10*, 1931–1943.
5. Seidel, Y. E.; Schneider, A.; Jusys, Z.; Wickman, B.; Kasemo, B.; Behm, R. J. Mesoscopic Mass Transport Effects in Electrocatalytic Processes. *Faraday Discuss.* **2008,** *140*, 167–184.
6. Seidel, Y. E.; Jusys, Z.; Wickman, B.; Kasemo, B.; Behm, R. J. Mesoscopic Transport Effects in Electrocatalytic Reactions. *ECS Trans.* **2010,** *25*, 91–102.
7. Seidel, Y. E.; Schneider, A.; Jusys, Z.; Wickman, B.; Kasemo, B.; Behm, R. J. Transport Effects in the Electrooxidation of Methanol Studied on Nanostructured Pt/Glassy Carbon Electrodes. *Langmuir* **2010,** *26*, 3569–3578.
8. Seidel, Y. E.; Jusys, Z.; Lindström, R.; Stenfeldt, M.; Kasemo, B.; Krischer, K. Oscillatory Behaviour in Galvanostatic Formaldehyde Oxidation on Nanostructured Pt/Glassy Carbon Model Electrodes. *Chem. Phys. Chem.* **2010,** *11*, 1405–1415.
9. Lindström, R.; Seidel, Y. E.; Jusys, Z.; Gustavsson, M.; Kasemo, B.; Behm, R. J. Electrocatalysis and Transport Effects on Nanostructured Pt/GC Electrodes. *J. Electroanal. Chem.* **2010,** *644*, 90–102.
10. Thomas, J. M.; Thomas, W. J. *Principles and Practice of Heterogeneous Catalysis*; VCH: Weinheim, Germany, 1997.
11. Long, J. W.; Stroud, R. M.; Swider, K. E.; Rolison, D. R. How to Make Electrocatayst More Active for Direct Methanol Oxidation—Avoid PtRu Bimetallic Alloys. *J. Phys. Chem. B* **2000,** *104*, 9772–9776.
12. Dubau, L.; Hahn, F.; Coutanceau, C.; Léger, J.-M.; Lamy, C. On the Structure effects of Bimetallic PtRu Electrocatalysts towards Methanol Oxidation. *J. Electroanal. Chem.* **2003,** *554−555*, 407–415.
13. Kaiser, J.; Colmenares, L.; Jusys, Z.; Mörtel, R.; Bönnemann, H.; Köhl, G.; Modrow, H.; Hormes, J.; Behm, R. J. On the Role of Reactant Transport and (Surface) Alloy Formation for the CO Tolerance of Carbon Supported PtRu Polymer Electrolyte Fuel Cell Catalysts. *Fuel Cells* **2005,** *6*, 190–202.
14. Basnayake, R.; Li, Z.; Katar, S.; Zhou, W.; Rivera, H.; Smotkin, E. S.; Casadonte, D. J., Jr.; Korzeniewski, C. PtRu Nanoparticle Electrocatalyst with Bulk Alloy Properties Prepared through a Sonochemical Method. *Langmuir* **2006,** *22*, 10446–10450.
15. Inoue, M.; Nishima, T.; Akamaru, S.; Taguchi, A.; Umeda, M.; Abe, T. CO Oxidation on Non-Alloyed Pt and Ru Electrocatalysts Prepared by the Polygonal Barrel-Sputtering Method. *Electrochim. Acta* **2009,** *54*, 4764–4771.
16. Roth, C.; Benker, N.; Theissmann, R.; Nichols, R. J.; Schiffrin, D. J. Bifunctional Electrocatalysis in Pt−Ru Nanoparticle Systems. *Langmuir* **2008,** *24*, 2191–2199.
17. Petrii, O. A. Pt−Ru Electrocatalysts for Fuel Cells: A Representative Review. *J. Solid State Electrochem.* **2008,** *12*, 609–642.
18. Fredriksson, H.; Alaverdyan, Y.; Dmitiev, A.; Langhammer, C.; Sutherland, D. S.; Zäch, M.; Kasemo, B. Hole-Mask Colloidal Lithography. *Adv. Mater.* **2007,** *19*, 4297–4306.
19. Fredriksson, H.; Chakarov, D.; Kasemo, B. Patterning of Highly Oriented Pyrolytic Graphite and Glassy Carbon Surfaces by Nanolithography and Oxygen Plasma Etching. *Carbon* **2009,** *47*, 1335–1342.
20. Biegler, T.; Rand, D. A. J.; Woods, R. Limiting Oxygen Coverage on Platinized Platinum; Relevance to Determination of Real Platinum Area by Hydrogen Adsorption. *J. Electroanal. Chem.* **1971,** *29*, 269–277.
21. Takasu, Y.; Iwazaki, T.; Sugimoto, W.; Murakami, Y. Size Effects of Platinum Particles on the Electro-oxidation of Methanol in an Aqueous Solution of $HClO_4$. *Electrochem. Commun.* **2000,** *2*, 671–674.
22. Cherstiouk, O. V.; Simonov, P. A.; Zaikowskii, V. I.; Savinova, E. R. CO Monolayer Oxidation at Pt Nanoparticles Supported

on Glassy Carbon Electrodes. *J. Electroanal. Chem.* **2003,** *554−555*, 241–251.

23. Gasteiger, H. A.; Markovic, N.; Ross, P. N.; Cairns, E. J. CO Electro-Oxidation on Well-Characterized Pt−Ru Alloys. *J. Phys. Chem.* **1994,** *98*, 617–625.

24. Wang, J. X.; Marinkovíc, N. S.; Zajonz, H.; Adzic, R. R. *In-Situ* X-Ray Reflectivity and Voltammetric Study of Ru(0001) Surface Oxidation in Electrolyte Solutions. *J. Phys. Chem. B* **2001,** *105*, 2809–2814.

25. Willsau, J.; Heitbaum, J. Analysis of Adsorbed Intermediates and Determination of Surface Potential Shifts by DEMS. *Electrochim. Acta* **1986,** *31*, 943–948.

26. Schmiemann, U.; Baltruschat, H. The Adsorption of Ethene at Pt Single Crystal Electrodes. Desorption Products and Observation of Multiple Adsorption States by DEMS. *J. Electroanal. Chem.* **1992,** *340*, 357–363.

27. Baltruschat, H. Differential Electrochemical Mass Spectrometry. *J. Am. Soc. Mass Spectrom.* **2004,** *15*, 1693–1706.

28. Weaver, M. J.; Chang, S. C.; Leung, L. W. H.; Jiang, X.; Rubel, M.; Szklarczyk, M.; Zurawski, D.; Wieckowski, A. Evaluation of Absolute Saturation Coverages of Carbon Monoxide on Ordered Low-Index Platinum and Rhodium Electrodes. *J. Electroanal. Chem.* **1992,** *327*, 247–260.

29. Jusys, Z.; Kaiser, J.; Behm, R. J. Electro-Oxidation of CO and $H_2$/CO Mixtures on a Carbon Supported Pt Catalyst— A Kinetic and Mechanistic Study by Differential Electrochemical Mass Spectrometry. *Phys. Chem. Chem. Phys.* **2001,** *3*, 4650–4660.

30. Zei, M. S.; Lei, T.; Ertl, G. Spontaneous and Electrodeposition of Pt on Ru(0001). *Z. Phys. Chem.* **2003,** *217*, 447–458.

31. Lei, T.; Zei, M. S.; Ertl, G. Electrocatalytic Oxidation of CO on Pt-Modified Ru(0001)Electrodes. *Surf. Sci.* **2005,** *581*, 142–154.

32. Alves, O. B; Hoster, H. E.; Behm, R. J. Electrochemistry at Ru (0001) in a flowing CO-saturated electrolyte–reactive and inert adlayer phases. *Phys. Chem. Chem. Phys.* **2011,** *13*, 6010–6021.

33. Gutierrez, C.; Caram, J. A. *In-Situ* Spectroscopic Study of the Adsorption of Carbon Monoxide on a Polycrystalline Ruthenium Electrode by EMIRS and PMRS. *J. Electroanal. Chem.* **1991,** *305*, 289–299.

34. Jusys, Z.; Kaiser, J.; Behm, R. J. Composition and Activity of High Surface Area PtRu Catalysts towards Adsorbed CO and Methanol Electro-oxidation. A DEMS Study. *Electrochim. Acta* **2002,** *47*, 3693–3706.

35. Koper, M. T. M.; Jansen, A. P. J.; van Santen, R. A. Monte Carlo Simulations of a Simple Model for the Electrocatalytic CO Oxidation on Platinum. *J. Chem. Phys.* **1998,** *109*, 6051.

36. Zhdanov, V. P.; Kasemo, B. Simulation of CO Oxidation on nm-Sized Supported Pt Particles: Stripping Voltammetry. *Chem. Phys. Lett.* **2003,** *376*, 220–225.

37. Vidakovic, T.; Christov, M.; Sundmacher, K. A Method for Rough Estimation of the Catalyst Surface Area in a Fuel Cell. *J. Appl. Electrochem.* **2009,** *39*, 213–225.

38. Jusys, Z.; Schmidt, T. J.; Dubau, L.; Lasch, K.; Jörissen, L.; Garche, J.; Behm, R. J. Activity of PtRuMeOx (Me = W, Mo or V) Catalysts towards Methanol Oxidation and their Characterization. *J. Power Sources* **2002,** *105*, 297–304.

39. Maillard, F.; Lu, G.-Q.; Wieckowski, A.; Stimming, U. Ru-Decorated Pt Surfaces as Model Fuel Cell Electrocatalysts for CO Electro-oxidation. *J. Phys. Chem. B* **2005,** *109*, 16230–16243.

40. Godoi, D. R. M.; Perez, J.; Villulas, H. M. Effects of Alloyed and Oxide Phases on Methanol Oxidation of Pt-Ru/C Nanocatalysts of the Same Particle Size. *J. Phys. Chem. C* **2009,** *113*, 8518–8525.

41. Sugawara, Y.; Yadav, A. P.; Nishikata, A.; Tsuru, T. EQCM Study on Dissolution of Ruthenium in Sulfuric Acid. *J. Electrochem. Soc.* **2008,** *155*, B897–B902.

42. Spendelow, J. S.; Babu, P. K.; Wieckowski, A. Electrocatalytic Oxidation of Carbon Monoxide and Methanol on Platinum Surfaces Decorated with Ruthenium. *Curr. Opinion Solid State Mater. Sci.* **2005,** *9*, 37–48.

43. Davies, J. C.; Hayden, B. E.; Pegg, D. J.; Rendall, M. E. The Electro-oxidation of Carbon Monoxide on Ruthenium Modified Pt(111). *Surf. Sci.* **2002,** *496*, 110–120.

44. Weber, S. G.; Long, J. T. Detection Limits and Selectivity in Electrochemical Detectors. *Anal. Chem.* **1988,** *60*, 903A–913A.

45. Bard, A. J.; Faulkner, L. R. *Electrochemical Methods— Fundamentals and Applications*, 2nd ed.; John Wiley & Sons: New York, 2001; 1−833.

46. Chen, S.; Kucernak, A. Electrocatalysis under Conditions of High Mass Transport: Investigation of Hydrogen Oxidation on Single Submicron Pt Particles Supported on Carbon. *J. Phys. Chem. B* **2004,** *108*, 13984–13994.

47. Chen, S.; Kucernak, A. Electrocatalysis under Conditions of High Mass Transport Rate: Oxygen Reduction on Single Submicrometer-Sized Pt Particles Supported on Carbon. *J. Phys. Chem. B* **2004,** *108*, 3262–3276.

48. Morf, W. E. Theoretical Treatment of the Amperometric Current Response of Multiple Microelectrode Arrays. *Anal. Chim. Acta* **1996,** *330*, 139–149.

49. Morf, W. E. Theoretical Treatment of the Current vs. Time Response of Microelectrode Arrays to Changes of Potential, Concentration, or Flow. *Anal. Chim. Acta* **1997,** *341*, 121–127.

50. Morf, W. E.; Koudelka-Hep, M.; de Rooij, N. F. Theoretical Treatment and Computer Simulation of Microelectrode Arrays. *J. Electroanal. Chem.* **2006,** *590*, 47–56.

51. Dickinson, E. J. F.; Streeter, I.; Compton, R. G. Chronoamperometry and Cyclic Voltammetry at Conical Electrodes, Microelectrodes, and Electrode Arrays: Theory. *J. Phys. Chem. B* **2008,** *112*, 4059–4066.

52. Schwechten, H., Heinen, M., Seidel, Y. E., Jusys, Z., Wickman, B., Kasemo, B., Behm, R. J., submitted for publication.

53. Alonso-Vante, N. Platinum and Nonplatinum Nanomaterials for the Molecular Oxygen Reduction Reaction. *ChemPhysChem* **2010,** *11*, 2732–2744.

54. Wang, J. X.; Brankovic, S. R.; Zhu, Y.; Hanson, J. C.; Adzic, R. R. Kinetic Characterization of PtRu Fuel Cell Anode Catalysts Made by Spontaneous Pt Deposition on Ru Nanoparticles. *J. Electrochem. Soc.* **2003,** *150*, A1108–A1117.

55. Gasteiger, H. A.; Markovic, N. M.; Ross, P. N. The Electro-oxidation of CO and $H_2$/CO Mixtures on a Well-Characterized $Pt_3$Sn Electrode Surface. *J. Phys. Chem.* **1995,** *99*, 8945–8949.

56. Kinoshita, K.; Ross, P. N. Oxide Stability and Chemisorption Properties of Supported Ruthenium Electrocatalysts. *J. Electroanal. Chem.* **1977,** *78*, 313–318.

57. Lin, W.-F.; Zei, M. S.; Kim, Y. D.; Over, H.; Ertl, G. Electrochemical *versus* Gas-Phase Oxidation of Ru Single-Crystal Surfaces. *J. Phys. Chem. B* **2000,** *104*, 6040–6048.

58. El-Aziz, A. M.; Kibler, L. A. New Information about the Electrochemical Behaviour of Ru(0001) in Perchloric Acid Solutions. *Electrochem. Commun.* **2002,** *4*, 866–870.

59. Jin, J. M.; Lin, W. F.; Christensen, P. A. *In-Situ* FTIR Spectroscopic Studies of the Oxidation of CO Adsorbates on Ru(0001) Electrodes under Open Circuit Conditions. *J. Electroanal. Chem.* **2004,** *563*, 71–80.

60. Moulder, J. F.; Stickle, W. F.; Sobol, P. E.; Bomben, K. D. *Handbook of X-ray Photoelectron Spectroscopy*; Perkin Elmer Corp.: Eden Prairie, MN, 1992.

61. Jusys, Z.; Kaiser, J.; Behm, R. J. A Novel Thin-Layer Flow Cell Double-Disk Electrode Approach for Kinetic Studies on Supported Catalysts under Controlled Mass Transport Conditions. *Electrochim. Acta* **2004,** *49*, 1297–1305.